Received: 22 June 2022 | Revised: 13 December 2022 | Accepted: 24 January 2023

DOI: 10.1111/ffe.13958

ORIGINAL ARTICLE

FFEMS Fatigue & Fracture of Engineering Materials & Structures WILEY

Fatigue behavior and lifetime assessment of an austenitic stainless steel in the VHCF regime at ambient and elevated temperatures

Tim Schopf[1] | **Stefan Weihe**[1] | **Tobias Daniel**[2] | **Marek Smaga**[2] | **Tilmann Beck**[2]

[1]Materials Testing Institute (MPA), University of Stuttgart, Stuttgart, Germany

[2]Institute of Materials Science and Engineering (WKK), University of Kaiserslautern, Kaiserslautern, Germany

Correspondence
Tim Schopf, Materials Testing Institute (MPA), University of Stuttgart, Pfaffenwaldring 32, 70569 Stuttgart, Germany.
Email: tim.schopf@mpa.uni-stuttgart.de

Funding information
Federal Ministry for Economic Affairs and Energy (BMWi), Germany

Abstract

While the LCF behavior of austenitic steels used in nuclear power plants is already well investigated, the VHCF regime has not been characterized in detail so far. For this, fatigue tests on the metastable austenitic steel AISI 347/1.4550 were performed with a servo-hydraulic testing system at test frequencies up to 980 Hz and with an ultrasonic fatigue testing system at a test frequency of 20,000 Hz. To compare these test results to the ASME standard fatigue curve (total strain amplitude vs. load cycles to failure), a fictitious-elastic and an elastically plastic assessment method was used. The elaborated elastic–plastic assessment method generates good results, while a purely elastic assessment in the VHCF regime, commonly used in literature, leads to significantly nonconservative results. Moreover, phase transformation from metastable austenite into stable α′-martensite can take place, and no specimen failure occurs in the VHCF regime. Consequently, for this material, a real endurance limit exists.

KEYWORDS

ambient temperature, austenitic stainless steel, cyclic deformation behavior, elevated temperature, fatigue assessment, VHCF, α′-martensite

Highlights

- AISI 347 shows a significant plastic strain component in the VHCF regime.
- Elastic–plastic FE-analysis describe cyclic material behavior in the VHCF regime accurately.
- An elastic–plastic based calculation method was elaborated to be able to assess fatigue lifetime.
- Results of the assessment method show a good accordance to experimental tests and the ASME code fatigue curve.

This is an open access article under the terms of the Creative Commons Attribution License, which permits use, distribution and reproduction in any medium, provided the original work is properly cited.
© 2023 The Authors. *Fatigue & Fracture of Engineering Materials & Structures* published by John Wiley & Sons Ltd.

1 | INTRODUCTION

Reactor internals are subjected to thermomechanical fatigue induced by operational temperature transients and flow-induced vibrations as well as their combination at an operating load range between ambient temperature and ~300°C.[1] The combined action of the resulting complex loads induces low cycle (LCF, $N_f \leq 10^3$), high cycle (HCF $\leq 10^3$ $N_f \leq 10^7$), and even very high cycle (VHCF, $10^7 > N_f \leq 10^{10}$) fatigue and their interaction. Methodological gaps within the current design codes are due to a huge lack of experimental data in the VHCF regime[2] (see Figure 1). Additionally, mean data curves in design codes are based on total strain-controlled fatigue tests with a 25% load drop failure criterion. Therefore, the fatigue curves are provided as mathematical approaches (by using the Langer equation with tree variables) describing a total strain amplitude over number of load cycles correlation, but no strain-based assessment method for fatigue tests in the VHCF regime is available by now. These aspects gain in importance particularly in the context of long-term operation.[3] The work presented in this paper primarily aims at contributing to closing these mentioned gaps by generating a data and assessment basis for the fatigue behavior of austenitic stainless steel components—particularly reactor internals—of nuclear power plants (NPPs) at high and very high numbers of load cycles.

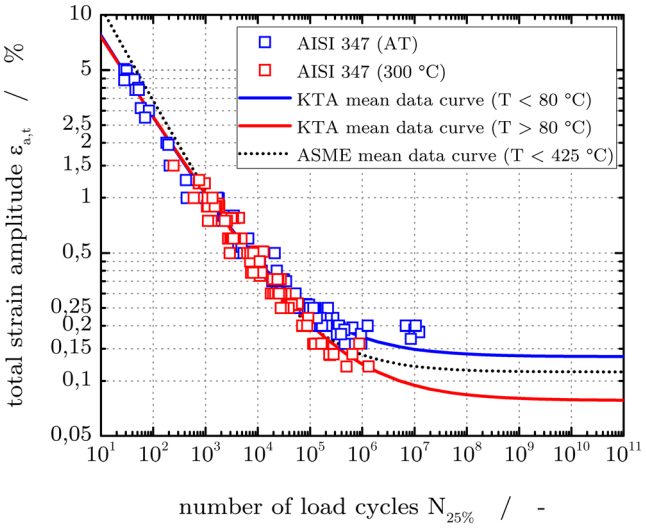

FIGURE 1 KTA (Germany: Kerntechnischer Ausschuss) data base for the austenitic stainless steel AISI 347 at ambient and elevated temperatures with the KTA and ASME (American Society of Mechanical Engineers) mean data curves.[2,4] [Colour figure can be viewed at wileyonlinelibrary.com]

To achieve highest load cycle numbers in the VHCF regime ($N \sim 10^9$) in an adequate test time, high-frequency fatigue testing systems are required. Using conventional servo-hydraulic systems operating usually at f = 5 Hz, fatigue tests up to 10^9 load cycles would take more than 5 years. In addition to resonance pulsators, which realize test frequencies up to 1000 Hz,[5] a servo-hydraulic system, which operates at up to 1000 Hz,[6] and above all ultrasonic fatigue systems[7,8] are used for VHCF investigations. Both a high-frequency servo-hydraulic test rig and an ultrasonic system are used in this work (see Section 3). While in conventional fatigue tests in the LCF and HCF regime, total strain control (Figure 2A) and stress measurement (Figure 2B) can be used to determine stress–strain hysteresis loops (Figure 2C) and to characterize the fatigue behavior, this is not possible for high-frequency systems in the same way. The servo-hydraulic high-frequency test system allows only stress-controlled tests without strain measurement (Figure 2D). In the case of the ultrasonic fatigue testing (USFT) system, the stress develops in a pulsed and displacement-controlled manner (Figure 2E). For an uniform representation of test results in a total strain amplitude over number of load cycles to failure ($\varepsilon_{a,t}$-N_f) curve from the LCF to the VHCF regime, a precise calculation of the total strain amplitude resulting in the VHCF tests is required. To determine the total strain amplitude for the stress-controlled tests on the servo-hydraulic system as well as from the displacement-controlled tests on the USFT system, an elastic–plastic assessment method was created for each case. These methods are adapted to the respective test principle and are based on the material behavior determined in total strain-controlled tests in the HCF and VHCF regime.

The abovementioned need for further research and development efforts is directly addressed by this paper. The fatigue behavior of technically important austenitic CrNi steels up to highest numbers of load cycles depends strongly on the austenite stability of the material.[9] While in stable austenite no phase transformation occurs due to cyclic loading, the cyclic deformation behavior of metastable face-centered cubic (fcc) γ-austenites is significantly affected by formation of the body-centered cubic (bcc) α′-martensite and twins.[10,11] These microstructural effects, which are influenced by the chemical composition, temperature, and stress or strain amplitude, lead to a cyclic hardening of the material, which results in a true fatigue limit, that is, no further decrease of the sustainable load amplitude in the VHCF regime.[9,12,13] In comparison, stable austenite and also metastable austenite with a high α′-martensite content in the initial state show a second decrease in fatigue life up to the highest numbers of load cycles.[11,14,15] The tendency of deformation-induced phase

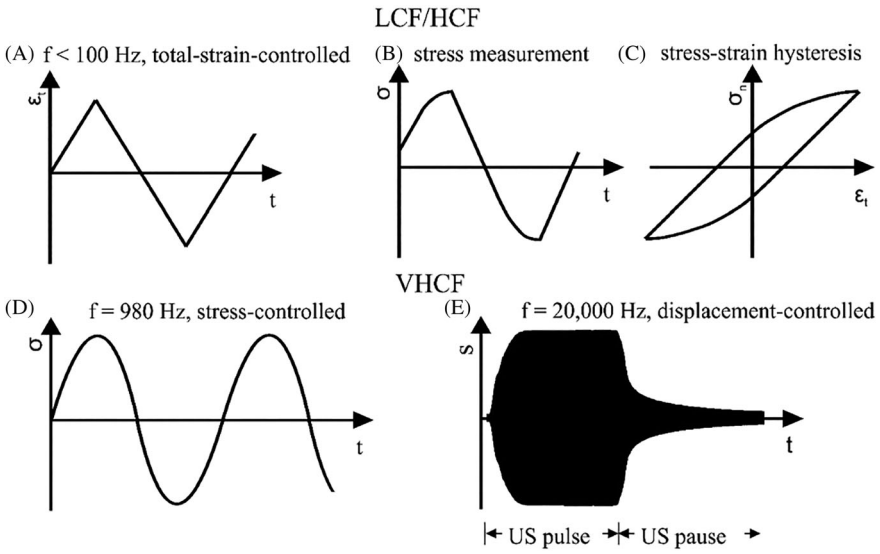

FIGURE 2 Schematic diagrams showing (A) ramped course of total strain-controlled loading, (B) respective stress response during elastic–plastic cyclic deformation and (C) resulting stress–strain hysteresis determined in LCF/HCF tests, (D) course of sinusoidal stress loading in a VHCF test using a high-frequency servo-hydraulic test system, and (E) pulsed displacement applied in an ultrasonic fatigue testing system.

TABLE 1 Chemical composition in wt% and austenite stability parameters of the investigated metastable austenitic steel AISI 347.

C	N	Cr	Ni	Nb	Mn	Mo	Si
0.04	0.007	17.6	10.64	0.62	1.83	0.29	0.41
M_S in °C		**M_{d30} in °C**			**SFE in mJ/m² at AT**		
−189		25			42		

transformation and twinning formation in metastable austenite decreases with increasing temperature,[11,16] so, especially at a typical operating temperature of 300°C, the characterization of the fatigue behavior of metastable austenitic steels is necessary. Due to the few results at ambient temperature in the VHCF regime and the hardly available results at elevated temperatures in the VHCF regime, further investigations up to the highest numbers of load cycles are needed for the design of austenitic components in NPPs.

2 | INVESTIGATED MATERIAL

The investigated material was the niobium stabilized metastable austenitic stainless steel AISI 347 (X6CrNiNb18-10, 1.4550). For the fatigue tests, specimens were extracted from an original nuclear power plant surge line pipe (archive material) with an outside diameter of 333 mm and a wall thickness of 36 mm. The pipe was manufactured seamless, drilled from the inside, turned from the outside, and delivered in a solution annealed state (1050°C/10 min), such that in the initial state, no α′-martensite was detected by microscopic, X-ray, and magnetic Feritscope™ measurements. Note that the surge line pipe was not previously used for applications in nuclear power plants. The chemical composition of the investigated material determined by spectral analysis is given in Table 1 and conforms to the limits given in the respective international standard. The aspect of metastability was evaluated on the basis of the widely accepted empirical parameters of M_S temperature according to Eichelmann,[17] $M_{d,30}$ temperature according to Angel,[18] and stacking fault energy.[16] The respective values given in Table 1 indicate a metastable state of the investigated material at ambient temperature.

The microstructure in the initial state was fully austenitic with typical annealing twins and relatively large grains (Figure 3A,B). Quantitative microstructure analysis by using planimetric method according to ASTM E112 showed a mean grain size of 120 µm without the consideration of solution annealing twins. All specimens of the investigated material for fatigue and tensile tests were mechanically and electrolytically polished to obtain a surface roughness of $R_z = 0.16$ µm and to remove small amounts of α′-martensite at the specimen surface that may have formed in the turning process. Afterward, magnetic Feritscope™ measurements on the specimens showed no ferromagnetic phase content $\xi = 0.00$ FE-%, confirming that no α′-martensite was present in the initial state.

The mechanical properties of the test material at ambient temperature and 300°C determined in each case from three tensile tests are shown in Table 2. The material shows a relation of good strength and ductility typical for austenitic materials. At ambient temperature, an α′-martensite content of $\xi = 4.41$ FE-% is formed up to failure, proving the metastable behavior described above. Note that ξ is the original measurement value from the magnetic Feritscope™ sensor, which correlates linearly with the ferromagnetic α′-martensite content.[19] Due to

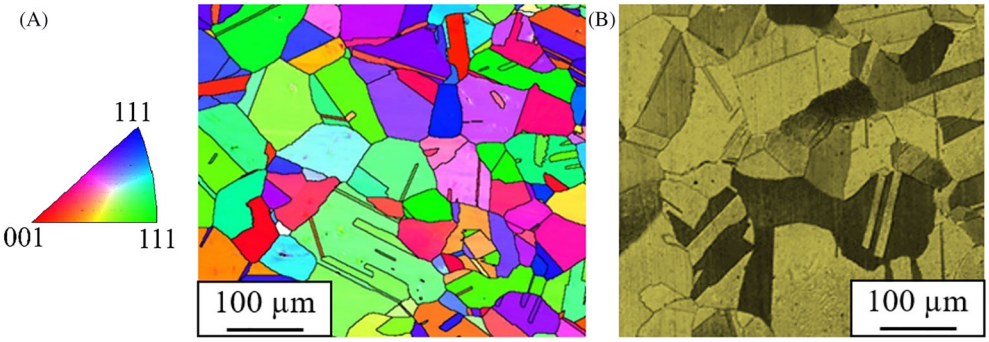

FIGURE 3 Microstructure in the initial state: (A) EBSD mapping and (B) light microscope image of a cross section. [Colour figure can be viewed at wileyonlinelibrary.com]

TABLE 2 Mechanical properties and α′-martensite content (ξ) after specimen failure.

	$R_{p0.2}$ in MPa	Young's modulus in GPa	UTS in MPa	A in %	ξ in FE-% after fracture
AT	242 ± 8	183 ± 9	569 ± 10	66 ± 2	4.41 ± 0.30
300°C	180 ± 2	159 ± 7	357 ± 3	36 ± 2	0.00 ± 0.00

the increased austenite stability at 300°C, no phase transformation takes place as a result of the quasi-static loading. As expected, an increase in temperature is accompanied by a decrease in Young's modulus as well as strength and elongation at fracture.

3 | EXPERIMENTAL SETUP

In this work three different strain rates/frequencies (1%/s, 980 Hz, 20 kHz) are applied during the fatigue tests in the LCF, HCF, and VHCF regime. Accordingly, the fatigue tests for this work were carried out on three different test rigs, which differ in test principle and control.

3.1 | LCF/HCF tests

Total strain-controlled fatigue tests with a strain rate of 1%/s were performed on a 100-kN Schenk servo-hydraulic test system. The strain measurement was realized by a clip gauge extensometer. In combination with the force recording by using a load cell, this setup allows determining stress–strain hysteresis for each individual load cycle (Figure 2A–C). For investigations at higher temperatures, an oven with multi-zone control was used. Therefore, a thermocouple, applied on the surface of the specimen, measures the temperature and controls the heating system within an accuracy of ±5 K.

3.2 | VHCF tests

To investigate the fatigue life in the VHCF regime, fatigue tests were performed on an ultrasonic fatigue testing system (UFTS) and on the high-frequency servo-hydraulic test rig MTS 1000 Hz[9] (Figure 2D).

The servo-hydraulic test system uses a voice coil servo valve, which allows stress-controlled fatigue testing at frequencies up to 980 Hz.[6] Due to the high frequency, it was not possible to record the strain and thus the stress–strain hysteresis on this system. Consequently, lifetime-oriented tests can be performed without information about the development of total and/or plastic strain. As a result of the continuous loading during this test, extreme heating of the specimen occurred within a short time,[20] so fatigue tests at 980 Hz and ambient temperature were not possible. Accordingly, the tests at this system were carried out at a temperature of 300°C by using an induction heating system from comp. TRUMPF Hüttinger. The induction generator with a nominal power of 5 kW is controlled by a type K thermocouple attached to the gauge length of the specimen. The temperature deviation during the tests at 300°C is ±2°C. Furthermore, a UFTS was used to perform tests at both ambient (AT) and elevated temperature with test frequencies of ∼20,000 Hz. The operating principle of the UFTS is based on the inverse piezoelectric effect.[21] For this, the converter transforms an electrical signal from the ultrasonic generator into a high-frequency mechanical oscillation. Using a booster, which amplifies the oscillation depending on its geometry, the mechanical oscillation is transferred to the specimen.[22,23]

All parts of the system were designed to assure that under resonance conditions, a standing wave develops along the load axis with a maximum displacement amplitude at the specimen ends and maximum stress–strain amplitude in the center of the gauge length of the specimen (see Figure 4). Due to the strong self-heating of the investigated material, the specimens were loaded in

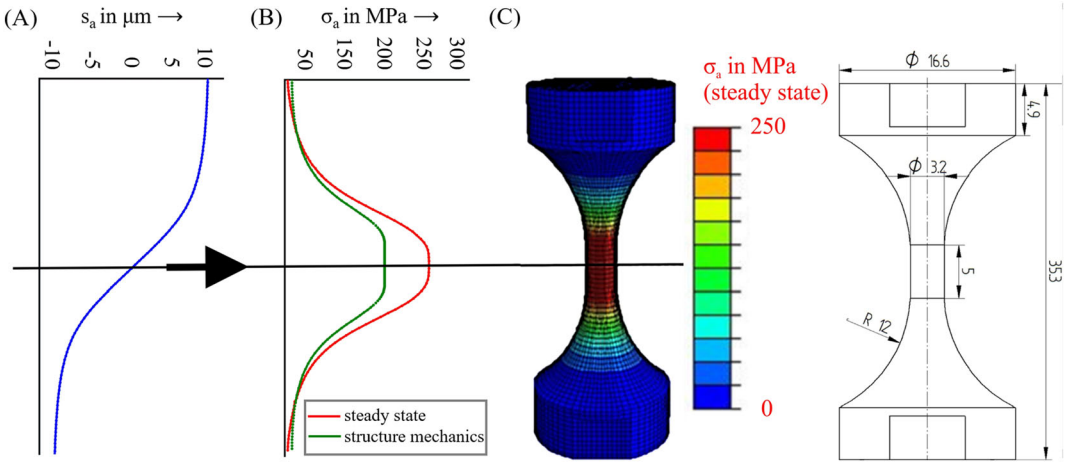

FIGURE 4 (A) Displacement distribution along the specimen axis during oscillation with a standing wave; (B) resulting stress profile along the specimen axis resulting from steady-state dynamic and structure mechanics analysis; (C) specimen shape and stress distribution with $s_a = 10$ µm at AT from steady-state dynamic analysis in ABAQUS. [Colour figure can be viewed at wileyonlinelibrary.com]

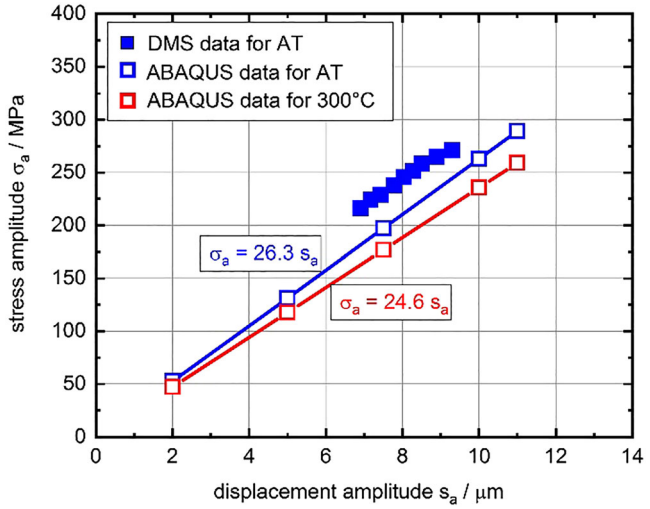

FIGURE 5 Relationship between stress amplitude–displacement amplitude taken from steady-state dynamic analysis in ABAQUS and strain gauge measurements. [Colour figure can be viewed at wileyonlinelibrary.com]

pulse-pause mode, which limits the maximum specimen temperature during cyclic loading.[24] Therefore, the generator power was increased rapidly at the beginning of the pulse sequence to achieve the desired displacement of the specimen measured by using a laser vibrometer. Then the power was regulated in such a way that the oscillation amplitude remains constant until the end of the pulse sequence before the generator power, and, hence, the displacement amplitude decreased to zero. The test was realized in such a manner that the displacement amplitudes during the pulses remain constant over the complete testing time.[22] No force measurement can be used to determine the stress–strain hysteresis in this test design, since no load cell can be integrated into the oscillation system. However, based on the maximum displacement that occurred at the top and bottom of the specimen (Figure 4A), the maximum stress that arises exactly in the center of the specimen's gauge length can be determined using finite element method (FEM) simulation of the steady vibration state in ABAQUS (red line in Figure 4B). Note that, opposed to the situation in conventional force-controlled fatigue testing where the stresses are homogeneously distributed over the complete gauge length, a rather pronounced stress peak occurs in the middle section of the VHCF specimen. The results of the FEM simulation were verified in tests with strain gauge measurements. The stresses determined from the strain using Hooke's law showed a deviation of max. 9% in the range of low stresses and of max. 6% in the range of higher stresses compared to the steady-state dynamic analysis (Figure 5). The material parameters, that is, Young's modulus, density and Poisson's ratio, used for the simulation are given in Table 3. Figure 4C visualizes the stress distribution in a 3D model along the load axis as well as the dimensions of the specimen.

In the following, the stress values from the steady-state dynamic simulation are used. The maximum stress amplitude calculated by a structural mechanics simulation (quasi-static analysis), considering elastic–plastic material behavior (see Section 4.1.2), shows a big difference compared to the steady-state dynamic simulation (green line in Figure 4B). Therefore, this method is not valid to calculate elastic–plastic stresses and strains due to ultrasonic fatigue tests. To address elastic–plastic material behavior even in the VHCF regime, a method was compiled based on steady-state dynamic analysis combined with a post-assessment considering elastic–plastic material behavior.

TABLE 3 Used parameters for the steady-state dynamic analysis.

	$R_{p0.2}$ [MPa]	Young's modulus [GPa]	UTS [MPa]	A [%]	ξ [FE-%]	ρ [g/cm³]	Poisson's ratio	Thermal conductivity μ [W/(m·K)]
AT	242	183	569	66	4.41	7.85	0.3	15
300°C	180	159	357	36	0.00	7.85	-	-

3.3 | Optical microscope

Optical microscopic investigations were performed on a Leica DM 6000 M optical microscope. The metallographic sections were first electrolytically polished and then etched with Beraha II to visualize the microstructure. The IMAGIC software used in this work provides various analysis options for determining the grain size and the phase fractions of multiphase materials.

3.4 | Feritscope™ measurements

To determine the α′-martensite content, ex situ magnetic Feritscope™ measurements were performed before and after the fatigue tests. Due to the higher permeability of the ferromagnetic α′-martensite compared to paramagnetic γ-austenite, the response of the material to magnetic induction increases with increasing ferromagnetic phase fraction.[19]

4 | RESULTS

4.1 | Numerical analysis and assessment methods

4.1.1 | Cyclic deformation behavior and VHCF material model

In the later on described assessment method, which considers elastic–plastic material behavior in the VHCF regime, numerical analyses are used as a fundamental. Therefore, the elastic–plastic material behavior has to be described accurately, and also, cyclic hardening and/or softening effects need to be considered. Hence, a material model based on Armstrong–Frederick and Chaboche (AFC) with a combined isotropic and kinematic hardening law was implement.[25,26] Valid material model parameters for the AISI 347 stainless steel, especially in the VHCF regime, cannot be found in the literature but have to be derived from experimental data like stress–strain hysteresis and from cyclic deformation curves. For more details about the model, see Daniel et al.[23] In the first step constant amplitude fatigue tests at several total strain amplitudes representing the different cyclic fatigue regimes were performed: (i) $\varepsilon_{a,t} = 0.2\%$ for HCF, (ii) $\varepsilon_{a,t} = 0.15\%$ for HCF/VHCF transition, and (iii) $\varepsilon_{a,t} = 0.1\%$ for VHCF. All tests were carried out with a constant strain rate of 1%/s. Stress–strain hysteresis loops were obtained from these experiments, which allows a detailed characterization of cyclic deformation behavior at ambient temperature (Figure 6A) and at 300°C (Figure 6B). The results clearly show that even the load amplitude $\varepsilon_{a,t} = 0.1\%$ (VHCF regime) leads to a significantly elastic–plastic material behavior at ambient temperature and at 300°C. Due to high cyclic hardening at AT, shown in Figure 7, the hysteresis at $\varepsilon_{a,t} = 0.2\%$ are plotted for different stages during lifetime to illustrate the evolution of the stress amplitude.

In order to estimate the $\varepsilon_{a,t}$–N_f curves, not only the relationship between stress and total strain but also the cyclic hardening and/or softening effects has to be considered since, at least in case of large total strain amplitudes, the investigated metastable austenitic steel does not show a stabilized stress–strain behavior. Experimental results at ambient temperature and at 300°C (Figure 7) indicate stable cyclic deformation behavior for load amplitudes in the VHCF regime ($\varepsilon_{a,t} = 0.10\%$) and only small changes in the resulting stress amplitude over the number of cycles for $\varepsilon_{a,t} = 0.15\%$ (HCF/VHCF transition regime). However, the cyclic loading with a total strain amplitude of $\varepsilon_{a,t} = 0.20\%$ (HCF regime) at ambient temperature leads to a significant increase of the stress amplitude until specimen failure (Figure 7A) due to pronounced α′-martensite formation. At 300°C, only a slight cyclic hardening was observed (Figure 7B). The material behavior, described in detail with the help of stress–strain hysteresis and cyclic deformation curves, serves as the basis for the numerical material model. Cyclic hardening effects are reproduced with phenomenological approaches and adapted by using mathematical methods and best-fit algorithms. Therefore, an AFC material model with three backstresses (Chaboche parameters C_{1-3}, γ_{1-3}) was applied (see Table 4), and for more details, see literature.[23,27,28] Plasticity initiates when stress passes over σ_{y0} (yield stress at zero plastic strain).

In addition to the characterization of the cyclic deformation behavior, microscopic investigations were carried out on longitudinal sections of two fatigued specimens

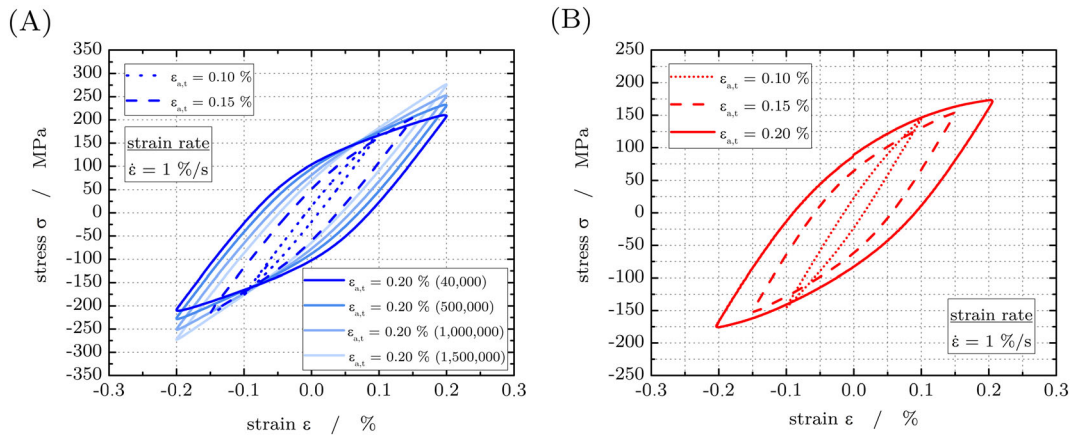

FIGURE 6 Representative stress–strain hysteresis for load levels in the HCF regime ($\varepsilon_{a,t} = 0.2\%$), the HCF/VHCF transition ($\varepsilon_{a,t} = 0.15\%$), and in the VHCF regime ($\varepsilon_{a,t} = 0.1\%$) at ambient temperature (A) and at T = 300°C (B). [Colour figure can be viewed at wileyonlinelibrary.com]

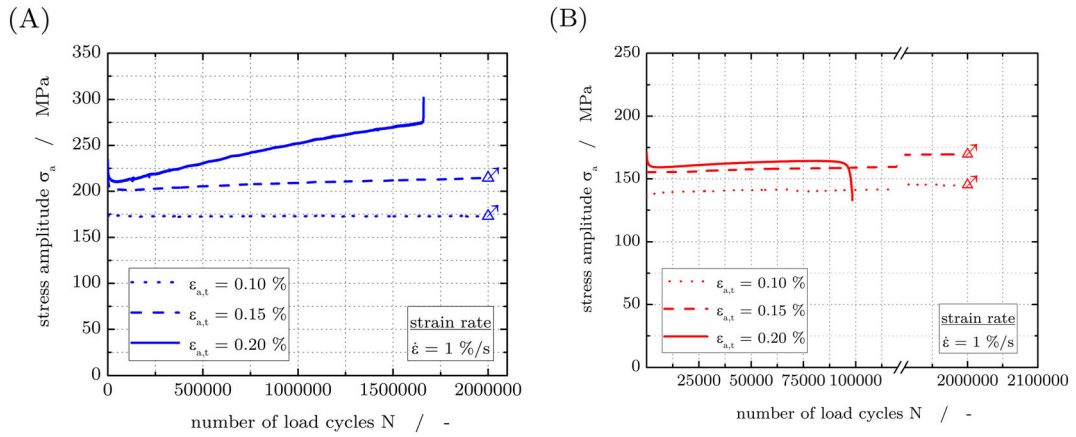

FIGURE 7 Cyclic deformation curves for fatigue tests in the HCF regime ($\varepsilon_{a,t} = 0.2\%$), the HCF–VHCF transition ($\varepsilon_{a,t} = 0.15\%$) and in the VHCF regime ($\varepsilon_{a,t} = 0.1\%$) at ambient temperature (A) and at 300°C (B). [Colour figure can be viewed at wileyonlinelibrary.com]

TABLE 4 Used parameters for the Armstrong–Frederick–Chaboche material model.

	σ_{y0}	C_1	γ_1	C_2	γ_2	C_3	γ_3
AT	120	143,140	1184	4256	0.474	4.057	172
300°C	80	416,270	5451	24,671	1.767	3043	235

after etching with Beraha II. Both specimens were loaded with $\varepsilon_{a,t} = 0.2\%$ and, hence, failed in the HCF regime, one at ambient temperature (Figure 8A,B) and the other at 300°C (Figure 8C,D). Figure 8A shows that deformation-induced α′-martensite formation occurs at ambient temperature, which results in a strong cyclic hardening (Figure 7A). The α′-martensite is rather homogeneously distributed over the entire gauge section, and its content decreases with increasing specimen diameter at the transition of the gauge section to the specimen shaft. The α′-martensite is present as blocks as well as points and needles. Magnetic Feritscope™ measurements indicated an average α′-martensite content of 10.5 FE-%. As described in Section 2, the austenite stability of the material increases with increasing temperature. As a result, the optical micrograph of the specimen fatigued at 300°C shows no α′-martensite (Figure 8D). Even at the tip of the failure crucial crack (Figure 8C) and the secondary crack (see Figure 8D), no α′-martensite can be detected. Accordingly, the magnetic Feritscope™ measurement indicates a ferromagnetic content of 0.0 FE-%.

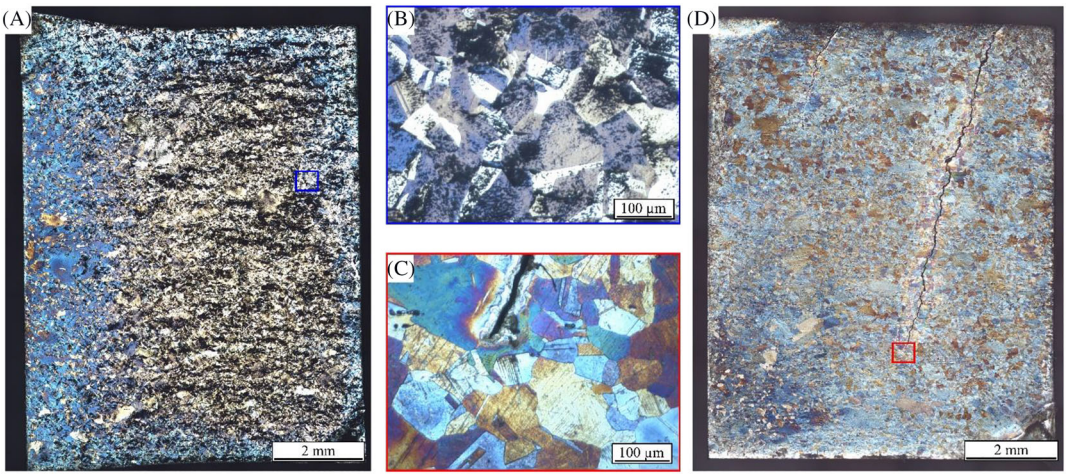

FIGURE 8 Optical microscopy of a specimen exposed to $\varepsilon_{a,t} = 0.2\%$ at ambient temperature, (A) overview and (B) detail, as well as at 300°C, (C) detail and (D) overview. [Colour figure can be viewed at wileyonlinelibrary.com]

4.1.2 | Elastic–plastic assessment methods

In order to establish a basis for comparison with the total strain amplitude–N curves obtained from total strain-controlled HCF tests, it is necessary to calculate the total strain amplitudes from the measured variables of the VHCF tests using a validated method. It is therefore of great importance in which way the tests are controlled and carried out since the technical implementation of the experiment defines the boundary conditions of the evaluation method. In this paper, VHCF tests were performed with a servo-hydraulic testing system and with an ultrasonic fatigue testing system. The test principles, described in detail in Section 3.1, differ fundamentally. For this reason, each of the two test principles requires its own evaluation method.

Assessment method for force-controlled fatigue tests

Servo-hydraulic systems contain an integrated load cell that allows direct measurement of the applied forces during the fatigue test. In principle, the attachment of an extensometer is possible for strain measurement and/or control. However, mechanical extensometry was not viable at frequencies of 980 Hz. For this reason, the tests were conducted in force control. Together with the specimen geometry and the test temperature, this information can be transferred into a numerical model. With the help of a simple 2D axisymmetric structural-mechanical simulation of the specimen, the test can be recalculated on the basis of the given boundary conditions using ABAQUS 2018. As further information material-specific parameters as Young's modulus, Poisson's ratio and Chaboche parameters of the material AISI 347 must be included in the numerical analysis. A subroutine assigns the appropriate parameter set on the basis of the stresses and

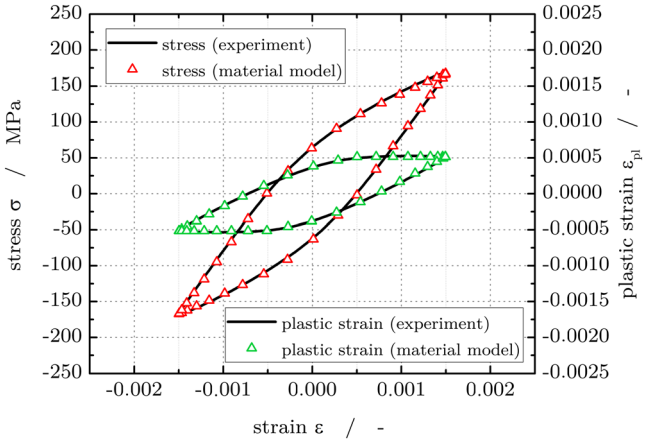

FIGURE 9 Comparison of the results for stress and plastic strain parts given from experimental data and numerical calculations using the described material model. [Colour figure can be viewed at wileyonlinelibrary.com]

temperatures that occur in order to transfer the elastic–plastic material behavior found in the experiment to the specimen in the numerical simulation. As a result, elastic and plastic strain components, described by the material model, show a good accordance to the experimental results (see Figure 9) and can therefore be calculated for every appearing load by simply using boundary conditions like displacements or forces.

Following the simulation, the stress and strain tensors can be read out for any time interval and at any location (node or Gauss point). These tensors describe the elastic–plastic stress–strain material behavior and, with a minimum–maximum consideration, allow a valid determination of the strain amplitude. As a result, an elastic–plastic strain amplitude is assigned to each experimentally determined number of load cycles and

a comparison with strain-controlled tests or standard curves is possible.

Assessment method for displacement controlled ultrasonic fatigue tests

The operating principle of an ultrasonic fatigue testing system differs from that of a servo-hydraulic system (see Section 2.1). The standing wave generated in the specimen causes a displacement on the lower and upper side of the specimen. Due to this working principle, the stress distribution within the specimen differs fundamentally from that obtained in conventional fatigue tests (see Figure 4B). As seen in Figure 5, the stresses generated by ultrasonic testing can be determined quite accurately by means of vibration analysis. For this purpose, a method based on elastic steady-state calculations combined with elastic–plastic post-assessment was elaborated. Therefore, it is necessary to build up a numerical model with all test-related boundary conditions and to evaluate it in a steady-state dynamic analysis at the operating frequency of UFTS (Figure 10A). Due to the principle of action, the stresses in the steady-state dynamic analysis are purely dependent on the elastic material properties. Hence, the steady-state dynamic analysis delivers the calculated maximum stress amplitude (Figure 10B). In addition, a cyclic stress–strain curve is applied, which was derived from experimental data (see Figure 6). For this purpose, cyclically stabilized stress–strain values are plotted against each other and described using the Ramberg–Osgood fit. The cyclic strain hardening coefficient K′ and the cyclic strain hardening exponent n′ are sufficient to unambiguously define the course of the Ramberg–Osgood equation. As for the elastic–plastic material model, a separate formulation must be derived for the cyclic stress–strain curve for ambient temperature and T = 300°C each. Note that the α′-martensite formation at ambient temperature (Figure 7) is implicitly taken into account in the respective cyclic stress strain curve showing more pronounced hardening at AT compared with T = 300°C. If a significant cyclic hardening due to α′-martensite formation occurs in the experiment, the cyclic stress–strain curve shown in dashed line in Figure 10C applies. Considering the additional material hardening ensures that the correct elastic–plastic strain amplitude is assigned to the assessment process. With the calculated stress amplitude from the steady-state dynamic analysis (input variable at y-axis), the corresponding elastic–plastic strain amplitude (output variable at x-axis) can be read from the cyclic stress–strain curves (Figure 10C) by considering temperature and

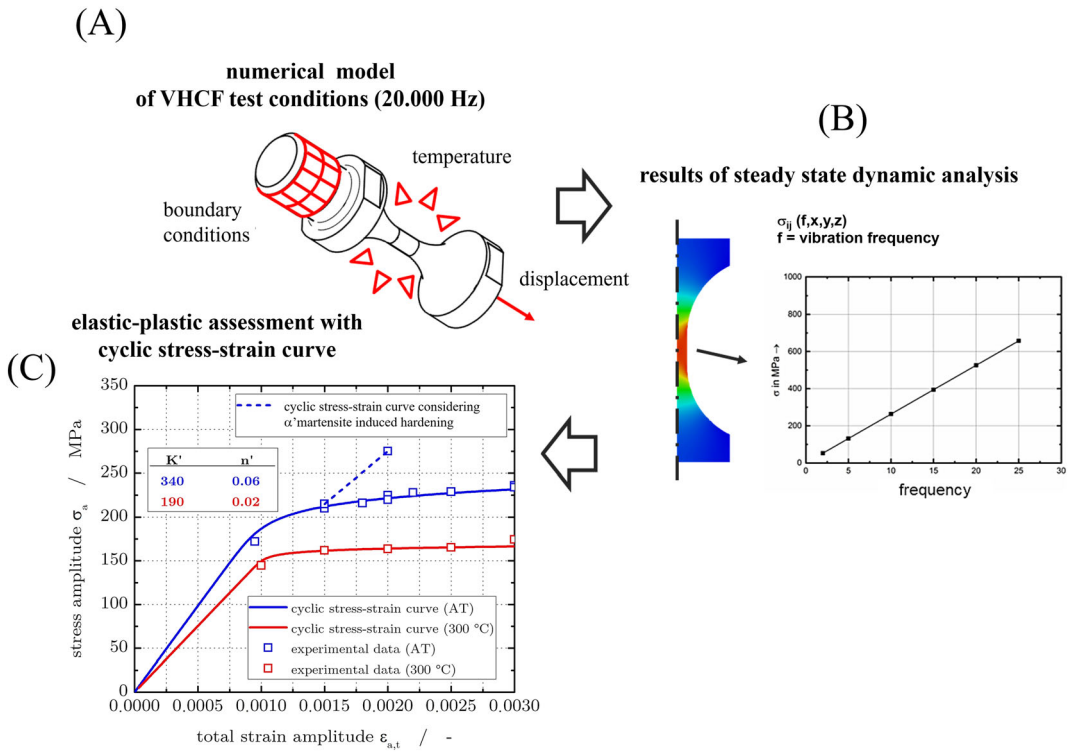

FIGURE 10 Cyclic stress–strain-curves at ambient temperature (considering cyclic hardening caused by α′-martensite formation) and elevated temperature in the HCF and VHCF regimes. (A) Numerical model of VHCF test conditions (20.000 Hz). (B) Results of steady-state dynamic analysis. (C) Elastic–plastic assessment with cyclic stress–strain curve. [Colour figure can be viewed at wileyonlinelibrary.com]

α′-martensite formation. As calculated forces in the specimen of the elastic steady-state dynamic analysis are valid due to considered dynamics and stiffness, applying these forces to an elastic–plastic structural–mechanical simulation would lead to the same stress magnitude in the middle cross section of the specimen but to the associated elastic–plastic strain. Therefore, going straight from the stresses of the steady-state dynamic analysis to the cyclic stress–strain-curve is a shortcut, and as a result, an elastic–plastic strain amplitude can be assigned to an experimentally determined number of load cycles. Thus, a comparison with strain-controlled tests and the standard fatigue curves (e.g., KTA[2] or ASME[4]) is possible and shows a good accordance (see Section 4.2).

4.2 | Fatigue life calculation

As already mentioned, a broad data basis in the HCF and VHCF series is to be established for the austenitic steel AISI 347. For this purpose, tests were carried out at ambient temperature and 300°C with test frequencies of 980 Hz and 20,000 Hz. Thus, tests up to a load cycle number of 2×10^9 could be performed within economically reasonable limits. The purely elastically evaluated stress amplitudes from the ultrasonic tests (squares) and the measured stresses from servo-hydraulic tests (stars) are plotted against the number of load cycles in Figure 11; run-outs are marked with an arrow. For both temperatures, a true fatigue limit is found below which no specimen failure occurred. The results presented in this work are in very good agreement with other results from literature, considering the metastability of austenitic steels. At ambient temperature (Figure 11A), two metastable steels AISI 304 and 347 show failure only up to 10^7 and hence true fatigue life up to $2x10^9$. For stable AISI 904L failure in VHCF regime occurred.[14] Consequently, this material has a smaller endurance limit in comparison to metastable steel. For AISI 316L, two different behaviors were identified. The AISI 316L investigated by Grigorgescu et al shows similar behavior as the metastable AISI 304 and 347, because in this case the AISI 316L is also metastable.[11] In contrast, another charge of AISI 316L investigated by Takashi et al[29] shows a continuously degrease of fatigue strength also in the VHCF regime, which indicated the stable state of austenite. For tests at elevated temperatures the fatigue life database of austenitic stainless steels series 3xx is small. However, the results form Takashi et al[29] are in good agreement with our work.

The results shown in Figure 12 have been calculated using the assessment concepts described in Section 4.1. In both diagrams, ambient temperature (Figure 12A) and 300°C (Figure 12B), the fictitious-elastic results are additionally shown as a basis for comparison. In both charts can be seen that experimental results in the VHCF regime for the AISI 347 assessed with a fictitious-elastic method are not valid because the material shows significant cyclic plasticity (see Figure 6). For this reason, the data points are far on the conservative side in terms of fatigue life and fatigue strength. At ambient temperature, the KTA and ASME mean data curves are way too conservative. By using best-fit algorithms and a lower limiting curve approach, new proposals are made by MPA fatigue curves based on the Langer equation to cover the data in the HCF regime and the endurance limit. For T = 300°C, a comparison with the mean data curve given by the ASME code shows that the elastic–plastic evaluation methods lead to a good agreement. The previous assumptions and curves based on extrapolation in the

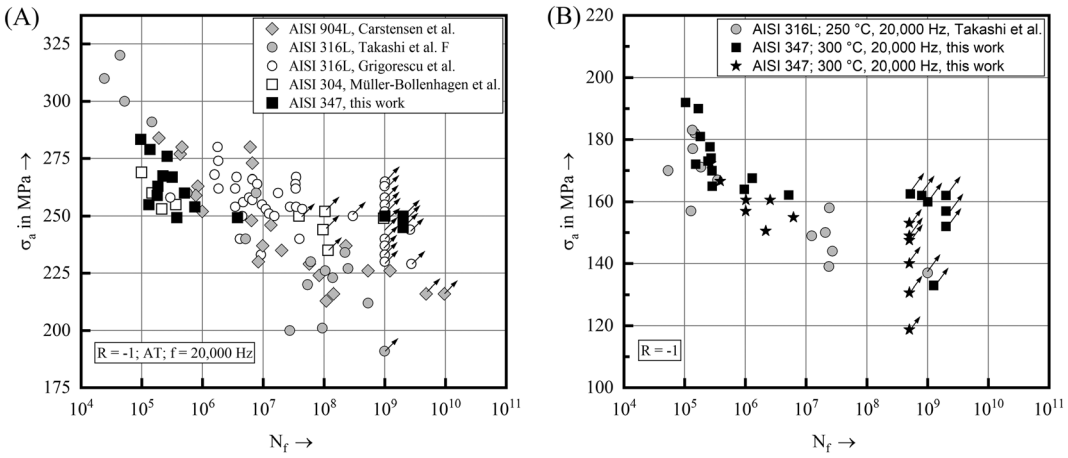

FIGURE 11 Fatigue life of austenitic stainless steels at ambient (A) and elevated temperature (B). The stress amplitude was determined by fictitious-elastic analysis.

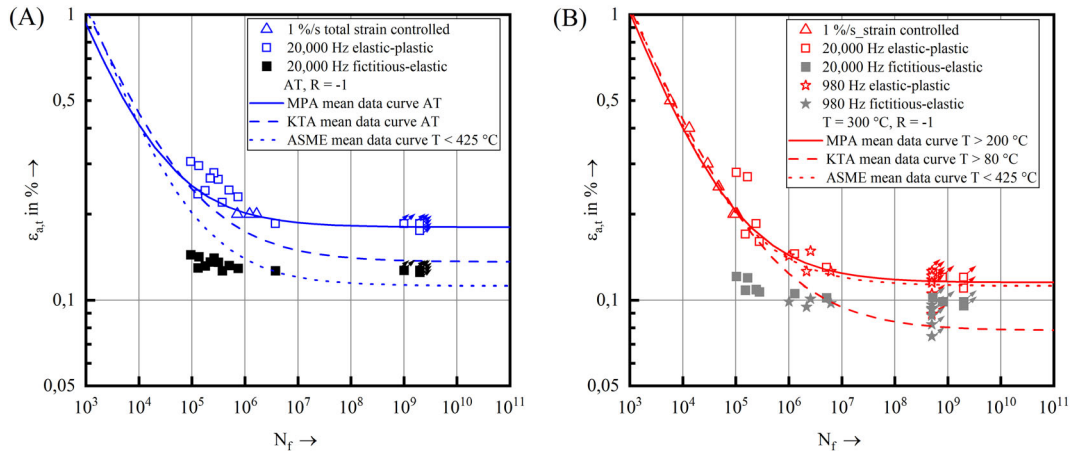

FIGURE 12 Calculation of a total strain amplitude fatigue life curve with a fictitious-elastic assessment method and with the elastic–plastic VHCF material model (A) at ambient temperature and (B) at 300°C.[2,4] [Colour figure can be viewed at wileyonlinelibrary.com]

VHCF regime could thus be validated experimentally. This not only describes the relationship between stress level and service life in the HCF and VHCF regime but also makes it possible to quantitatively determine a fatigue limit for ambient temperature and at an operationally relevant temperature of 300°C.

5 | SUMMARY AND CONCLUSIONS

It has been shown that for metastable austenitic steels with an elastic–plastic material behavior in the VHCF regime, the "state of the art" assessment approach, that is, a fictitious-elastic assessment, leads to insufficient and highly non-conservative results. Within this paper, a data and assessment basis for the fatigue behavior of the austenitic stainless steel AISI 347 at high and very high numbers of load cycles was elaborated. Therefore, fatigue tests in the HCF and VHCF regime were performed up to a load cycle number of 2×10^9 and at frequencies of 980 Hz and 20,000 Hz. Since there is no possibility to measure stress–strain hysteresis during these high-frequency tests, assessment methods are introduced to consider elastic–plastic material behavior. The results show that at ambient temperature, the mean data curves of nuclear codes such as the KTA and ASME are designed to be extremely conservative in the VHCF regime. At elevated temperatures of $T = 300°C$, the ASME code shows a good accordance with the assessed experimental results in the HCF and VHCF regime. For both temperatures, a new mean data curve was proposed that covers the entire database and takes the endurance limit into account.

AUTHOR CONTRIBUTIONS

Tim Schopf and Tobias Daniel carried out the experiments, performed the numerical simulations, and drafted the manuscript. Marek Smaga had oversight for the research work at WKK and helped to draft the manuscript. Stefan Weihe and Tilman Beck supported as expert adviser, mentor, and specifically critical reviewer. All authors read and approved the final manuscript.

ACKNOWLEDGEMENTS

The authors thank the Federal Ministry for Economic Affairs and Energy (BMWi), Germany, for the financial support. Open Access funding enabled and organized by Projekt DEAL.

DATA AVAILABILITY STATEMENT

The data that support the findings of this study are available from the corresponding author upon reasonable request.

REFERENCES

1. Chopra OK, Shack WJ. Effect of LWR Coolant Environments on the fatigue life of reactor materials. *Final Report, NUREG/CR-6909, Rev. 1*, U.S. Nuclear Regulatory Commission, 2018.
2. KTA 3201: components of the reactor coolant pressure boundary of light water reactors. Part 2: design and analysis, *German Nuclear Safety Standard*, Ed. 2017.
3. KTA 3204: reactor pressure vessel internals, *German Nuclear Safety Standard*, Ed. 2017-11, p. 39.
4. ASME Boiler & Pressure Vessel Code. Section III, division 1 – subsection NB: class 1 components, rules for construction of nuclear power plant components, The American Society of Mechanical Engineers, 2019.
5. Berchtold M, Klopfer I. Fatigue testing at 1000Hz testing frequency. *Procedia Struct Integr*. 2019;18:532-537.

6. Morgan JM, Milligan WW. A 1 kHz servohydraulic fatigue testing system. In: *Proceeding High Cycle Fatigue of Structural Materials*. Springer; 1997:305-312.
7. Bathias C. Piezoelectric fatigue testing machines and devices. *Int J Fatigue*. 2006;28(11):1438-1445.
8. Stanzl-Tschegg S. Very high cycle fatigue measuring techniques. *Int J Fatigue*. 2014;60(2014):2-17, Elsevier.
9. Smaga M, Boemke A, Daniel T. Fatigue behavior of metastable austenitic stainless steels in LCF, HCF and VHCF regimes at ambient and elevated temperatures. *Metals*. 2019;9(6):704.
10. Müller-Bollenhagen C. Verformungsinduzierte Martensitbildung mehrstufiger Umformung und deren Nutzung zur Optimierung der HCF- und VHCF-Eigenschaften von austenitischem Edelstahlblech. Siegener Werkstoffkundliche Berichte, 03-2011, 2011.
11. Grigorescu A, Hilgendorff P-M, Zimmermann M, Fritzen C-P, Christ H-J. Fatigue behavior of austenitic stainless steels in the VHCF regime. In: Christ H-J, ed. *Fatigue of Materials at Very High Numbers of Loading Cycles*. Springer; 2018:49-72.
12. Zimmermann, M.; Grigorescu, A.; Müller-Bollenhagen, C.; Christ, H.-J.: Influence of deformation-induced alpha prime martensite on the crack initiation mechanism in a metastable austenitic steel in the HCF and VHCF regime. *Proc. 13th Conference. on Fracture* (2013), pp. 5208-5216.
13. Daniel T, Smaga M, Beck T. Cyclic deformation behavior of metastable austenitic stainless steel AISI 347 in the VHCF regime at ambient temperature and 300 °C. *Int J Fatigue*. 2022; 156:106632.
14. Carstensen JV, Mayer H, Brondsted P. Very high cycle regime fatigue of thin walled tubes made from austenitic stainless steel. *Fatigue Fract Eng Mater Struct*. 2002;25(8-9):837-844.
15. Müller-Bollenhagen C, Zimmermann M, Christ H-J. Adjusting the very high cycle fatigue properties of a metastable austenitic stainless steel by means of the martensite content. *Proc Eng*. 2010;2(1):1663-1672.
16. Martin S, Fabrichnaya O, Rafaja D. Prediction of the local deformation mechanisms in metastable austenitic steels from the local concentration of the main alloying elements. *Mater Lett*. 2015;159:484-488.
17. Eichelmann GH, Hull FC. The effect of composition in the temperature of spontaneous transformation of austenite to martensite in 18-8 type stainless steel. *Trans ASM*. 1952;45: 77-104.
18. Angel T. Formation of martensite in austenitic stainless steels - effects of deformation, temperature and composition. *J Iron Steel Inst*. 1954;165-174.
19. Talonen J, Aspegren P, Hnninen H. Comparison of different methods for measuring strain induced α-martensite content in austenitic steels. *Mater Sci Technol*. 2004;20-12(12):1506-1512.
20. Daniel T, Boemke A, Smaga M. Investigations of very high cycle fatigue behavior of metastable austenitic steels using servohydraulic and ultrasonic testing systems. Proceeding ASME PVP Conference; 2018:PVP2018-PVP84639.
21. Curie J, Curie P. *Contractions et dilatations produites par des tensions electriques dans les cristaux hemiedres a faces inclines*. Vol. 93. Paris: Academic des sciences; 1881:1137-1340.
22. Daniel T, Smaga M, Beck T. *Ermüdungsverhalten des metastabilen austenitischen Stahls AISI 347 bei Raumtemperatur und 300°C im VHCF-Bereich*. Werkstoffprüfung; 2019:81-86.
23. Daniel T, Smaga M, Beck T, Schopf T, Stumpfrock L, Weihe S, Rudolph J. Investigation of the very high cycle fatigue (VHCF) behavior of austenitic stainless steels and their welds for reactor internals at ambient temperature and 300°C. Proceedings of the ASME PVP, 2020.
24. Müller T, Sander M. On the use of ultrasonic fatigue testing technique – variable amplitude loadings and crack growth monitoring. *Ultrasonics*. 2013;53(8):1417-1424.
25. Frederick C, Armstrong P. A mathematical representation of the multiaxial Bauschinger effect. *Mater High Temp*. 2007;24:1-26 reprint.
26. Chaboche JL. A review of some plasticity and viscoplasticity constitutive theories. *Int J Plast*. 2008;24(10):1642-1693.
27. Chaboche JL, Rousselier G. On the plastic and viscoplastic constitutive equations – part I: rules developed with internal variable concept. *J Press Vessel Technol*. 1983;105(2):153-158. ASME May 1983.
28. Dafalias Y, Kourousis K, Saridis G. Multiplicative AF kinematic hardening in plasticity. *Int J Solids Struct*. 2008;45:2861-2880, Elsevier Ltd.
29. Naoe T, Xiong Z, Futakawa M, Gigacycle fatigue behaviour of austenitic stainless steels used for mercury target vessels, Japan Atomic Energy Agency Institutional Repository.

How to cite this article: Schopf T, Weihe S, Daniel T, Smaga M, Beck T. Fatigue behavior and lifetime assessment of an austenitic stainless steel in the VHCF regime at ambient and elevated temperatures. *Fatigue Fract Eng Mater Struct*. 2023; 46(5):1763-1774. doi:10.1111/ffe.13958